Effect of Particle Size Distribution on Powder Packing and Sintering in Binder Jetting Additive Manufacturing of Metals

Yun Bai
Design, Research, and Education for Additive Manufacturing Systems Laboratory, Department of Mechanical Engineering, Virginia Tech, Blacksburg, VA 24061

Grady Wagner
Design, Research, and Education for Additive Manufacturing Systems Laboratory, Department of Mechanical Engineering, Virginia Tech, Blacksburg, VA 24061

Christopher B. Williams
Design, Research, and Education for Additive Manufacturing Systems Laboratory, Department of Mechanical Engineering, Virginia Tech, Blacksburg, VA 24061
e-mail: cbwill@vt.edu

The binder jetting additive manufacturing (AM) process provides an economical and scalable means of fabricating complex parts from a wide variety of materials. While it is often used to fabricate metal parts, it is typically challenging to fabricate full density parts without large degree of sintering shrinkage. This can be attributed to the inherently low green density and the constraint on powder particle size imposed by challenges in recoating fine powders. To address this issue, the authors explored the use of bimodal powder mixtures in the context of binder jetting of copper. A variety of bimodal powder mixtures of various particle diameters and mixing ratios were printed and sintered to study the impact of bimodal mixtures on the parts' density and shrinkage. It was discovered that, compared to parts printed with monosized fine powders, the use of bimodal powder mixtures improves the powder's packing density (8.2%) and flowability (10.5%), and increases the sintered density (4.0%) while also reducing the sintering shrinkage (6.4%). [DOI: 10.1115/1.4036640]

Keywords: additive manufacturing, 3D printing, binder jetting, sintering, powder metallurgy, copper

1 Introduction

1.1 Achieving Full Density—A Challenge in Binder Jetting of Metals. The binder jetting AM process can be used to fabricate metal parts by selectively inkjet printing a liquid binding agent into a powder bed, followed by postprocess sintering of the printed green part. As shown in Fig. 1, the jetted binder droplets interact with the powder particles to form primitives that stitch together to form a cross-sectional layer. Once a layer is printed, a new layer of powder is recoated on top of the previous layer, which is then printed and stitched to the previous layer by the jetted binder. The layer-by-layer process is repeated to create the complete green part. The unbound loose powder in the bed that surrounds the part supports overhanging structures during the build, and can be removed after printing via compressed air. Once depowdered, the green part is thermally treated to burn off the binder and sinter the powder particles together to obtain final density and strength.

As binder jetting of metals functionally separates part creation from powder sintering, the common processing challenges found in direct-metal additive manufacturing processes—such as the requirement of anchors and/or heat sinks added to the geometry—are avoided [1]. The ability to fabricate a metal part in a powder bed without the need for built anchors enables binder jetting to create large and geometrically complex parts without difficult postprocess cleaning. Binder Jetting is also an inherently scalable technology as it does not require an enclosed chamber and features high throughput enabled by the inkjet printing technology. In addition, as binder jetting does not use an energy beam to process material, it is well suited for optically reflective and thermally conductive metals, which can be challenging for powder bed fusion processes. For example, the feasibility of manufacturing high purity copper via binder jetting has been demonstrated in the authors' previous work [2].

The primary challenge in fabricating metal parts using binder jetting is in achieving a fully dense product following the sintering postprocess. Pores typically exist in sintered ceramics or metals fabricated in binder jetting [3,4]. For example, while the authors were able to create complex structures from copper powders in their prior work, the overall mechanical strength (116.7 MPa) is limited by the substantial porosity (15%) in sintered parts [2]. Porosity is challenging to eliminate during sintering because of a low powder bed density and the inability to process ultra-fine powders. Coarse powders are suitable for spreading and packing, but the large particles significantly inhibit sintering densification due to the low sintering driving force. Fine powders are preferred for sintering; however, the powder bed is typically poorly packed, and the powder recoating can be difficult due to powder's low flowability and agglomeration. As such, metal parts made by binder jetting are typically infiltrated with a lower melting point material in order to obtain full density.

Fabricating highly dense metal parts in binder jetting without infiltration has been a major focus for binder jetting research. Spray-dried granules and slurry-based powders have been used to overcome the difficulty to recoat fine powders [5,6]. A powder compaction mechanism has been developed to increase the powder packing density [7,8]. Liquid-phase sintering mechanism or

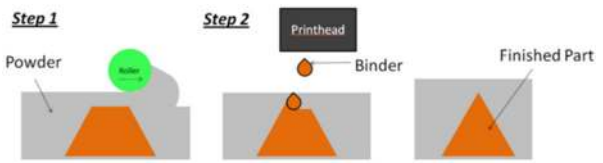

Fig. 1 Green part printing process in binder jetting (see figure online for color)

Manuscript received December 14, 2016; final manuscript received April 19, 2017; published online June 1, 2017. Assoc. Editor: Zhijian J. Pei.

optimized sintering parameters can also increase sintered density [3,9,10]. Pressure-assisted sintering has been demonstrated to be able to approach full density in binder jetting of ceramics [11].

1.2 Improving Sintered Density Via Bimodal Powder Mixtures. One well-established theory to improve powder packing and increase green density in powder processing techniques is using bimodal powder mixtures. The well-packed powder mixtures, wherein the small particles fill the interstitial voids between large particles, have many benefits such as (i) improved green part property (density and strength) and (ii) less shrinkage after sintering.

However, compared with the certainty and reliable prediction in improving the powder packing and green density by bimodal powder, the sintered density improvement is often complicated and uncertain. While small particles have rapid sintering rate and enhanced sintering stress [12], in bimodal powder mixtures, the added smaller particles typically bond to the large particles and offer little influence on the overall densification. The addition of coarse powders to a fine powder matrix may increase the packing density, but the difficulty to sinter large particles also hinders densification. German developed a prediction of sintered density of bimodal mixtures and validated with a series of experiments using various materials [13]. In this prediction, the sintered density improvement in a bimodal mixture is influenced by many factors including coarse-fine particle size ratio, powder constituents' packing density and sintering shrinkage, and powder mixing homogeneity. According to the bimodal powder sintering experiments known to the authors, fine powder constituent should be used rather than the bimodal mixture in order to achieve the maximum sintered density.

Particle size distribution and bimodal mixtures have been explored in powder-bed-based AM processes. The modeled powder bed formation process using discrete element method shows a dependency on layer thickness in predicting bimodal powder bed's packing density [14]. The experiments with bimodal powder has demonstrated capabilities of increasing layer density by 15% [15]; preventing balling phenomenon and achieving higher radiative heat flux in the powder bed [16]; and influencing final density and mechanical properties [17]. However, the study of sintering bimodal powder mixtures in the context of binder jetting of metals is limited. Lanzetta and Sachs studied the improved surface finish and printed primitive morphology in unfired bimodal powders parts [18]. Verlee et al. explored the sintered density of stainless steel bimodal mixtures; no improvement in sintered density was observed in the experiments [19].

1.3 Context. While the sintering experiments in the literature do not validate bimodal powder mixtures as an effective method to increase sintered density, it is hypothesized that in binder jetting the bimodal powder mixture has a greater potential to improve sintered density when compared with the coarse or fine powder constituents. Unlike traditional powder shaping methods, the poor flowability of fine powders in binder jetting inhibits achieving satisfactory powder bed packing and green density, which becomes a main obstacle in achieving fully dense parts. Bimodal powder mixture overcomes the poor powder packing of fine powder, and is capable of producing dense green parts that contain high sintering stress small particles, which may finally lead to an improved sintered density.

Additional benefits also exist in using bimodal powder mixture in binder jetting. As most metal parts in binder jetting undergo a large degree of shrinkage after sintering (without infiltration), there is a need to increase powder bed packing density to reduce shape distortion for a better product dimensional control. In addition, a powder mixture containing coarse powders typically lowers the powder cost as compared to a powder bed composed of solely fine powders.

The main research goals of this work are to (i) validate the hypothesis that bimodal powder mixtures can improve sintered part density in binder jetting, (ii) develop an understanding in the manufacturing process's influence on the relationship between particle size distribution and final green/sintered part property, and (iii) develop a framework in material property improvement through powder particle size optimization in binder jetting. To achieve these goals, the authors experimentally investigated the use of bimodal powder mixtures in binder jetting of copper. The experimental method is detailed in Sec. 2. A discussion of the results is provided in Sec. 3, and a closure is offered in Sec. 4.

2 Experimental Method

To explore the effects of bimodal powders on binder jetting's performance, the authors evaluated five mixtures (Sec. 2.1) on (i) powder bed density (Sec. 2.2), (ii) green and sintered part density, and (iii) part shrinkage (Sec. 2.5). In addition, the experiments were conducted to explore the impact of sintering conditions on powder mixtures (Sec. 2.4). The printing process parameters are detailed in (Sec. 2.3).

2.1 Powder Selection and Characterization. Binder jetting of metals inherently impose upper and lower limits of particle size selection in order to successfully recoat and sinter [20], therefore, the coarse-fine particle size ratio was explored in a small range in this work (1:3–1:6). Gas-atomized copper powders (over 99% purity) were chosen for easy recoating. The copper powders used for mixing are listed in Table 1 with particle size information. Five bimodal mixtures were created by mixing fine powder with coarse powder with 73–27 (a ratio that is efficient in maximizing powder packing density [21]) or 27–73 weight ratios. As the bimodal mixture has been extensively studied in the prior literature with a large variety of different coarse-fine powder mixing ratios, this work chose fewer mixing ratios to explore the uniqueness of sintering performance in binder jetting. Each mixture was mixed for 2 h in a rotating drum without media to ensure homogeneity. Laser scattering with a Horiba LA-950 was used to analyze particle size distribution (ASTM B822) of the powder mixtures.

2.2 Powder Packing Density Assessment. Powder apparent density, tap density, and powder bed density were measured for evaluating powder packing efficiencies. Apparent density, which should be the lower density threshold in binder jetting, was measured using a Hall flow meter (ASTM Standard 212). Tap density, which should be the upper threshold, was measured using a tapping apparatus (ASTM Standard 527). The ratio of apparent and tap density (Hausner ratio) was used to assess powder flowability (lower ratio corresponds to better flowability).

2.3 Printing Process Parameters. An ExOne R2 printer and solvent-based polymeric binder was used for all experiments; 18 mm × 6 mm × 3 mm test coupons were printed for density evaluations.

The layer thickness should be larger than the largest particle and is recommended to be at least three times of the particle diameter for higher packing density and smoother surface finish [20]. Given the powder size ranges from 5 μm to 75 μm, all samples were printed with 80–100 μm layer thickness (except for 150 μm thick layer for 75 μm powder). The counter-rotating roller spread powder with a constant speed of 5 mm/s to maintain a similar compaction effect across the tested powder mixtures.

Binder saturation ratio describes the amount of binder in the void space between powder particles (a detailed description of binder saturation variable is available in the authors' previous publication [2]). While 100% saturation ratio was used for all parts to obtain satisfactory printing quality, 150% was used for 5 μm powders, as its large total surface area requires extra binder for sufficient bonding. The measured apparent density (Sec. 2.2) was used for each powder to ensure accurate binder saturation.

The powder bed temperature was maintained at 80 °C during printing, and an overhead heater (185 °C) was used to dry each printed layer with a scanning speed of 5 mm/s.

Table 1 Copper powders used for creating mixtures

Powder name	D10 (10% particle pass diameter	D50 (median particle diameter)	D90 (90% particle pass diameter)
75 μm powder	58.0 μm	77.0 μm	101.5 μm
30 μm powder	15.0 μm	30.0 μm	37.5 μm
15 μm powder	8.0 μm	17.0 μm	28.0 μm
5 μm powder	0.65 μm	5.5 μm	9.0 μm

2.4 Postprocessing and Sintering. Sintering experiments were conducted in a tube furnace with atmosphere control. All sintering cycles used in this work feature a pure hydrogen atmosphere for copper oxide reduction and an isotherm at 450 °C for 30 min to facilitate debinding. Peak sintering temperature, duration, and heating rates were later altered to study the sintered density of bimodal mixtures under different sintering conditions (Sec. 3.3). Three samples were printed and sintered for each sintering condition.

2.5 Green and Sintered Part Characterization. The sintered density was measured by an immersion method with Archimedes principle following ASTM Standard 962. Green density, on the other hand, was calculated by the measured printed part weight and dimensions as the immersion method is not applicable to green parts printed with water-soluble binder.

An FEI Quanta 600 FEG Environmental scanning electron microscope (SEM) was used to examine the surface morphology of sintered parts. Sintered parts were also sectioned and polished for optical microscopy imaging to observe pore morphology and porosity.

3 Results and Discussion

3.1 Bimodal Powder Mixture's Impact on Powder Packing

3.1.1 Particle Size Distribution. The median particle size and standard deviation of the powder mixtures and their constituents are shown in Table 2. With the exception of the 75 + 15 powder, most powder mixtures exhibit expanded particle size deviation without discrete bimodal distribution. This can be explained by the insufficient large-to-small particle size ratio used in this work (3:1–6:1).

3.1.2 Measured Powder Density and Printed Part Green Density. Table 2 shows that the apparent/tap density in bimodal mixtures noticeably surpass the constituent powders. For example, after introducing a small portion of large particles to the 5 μm powder, the apparent density has improved by 12.7% (30 μm) and 5.6% (15 μm), and the tap density has improved by 5.6% (30 μm) and 4.9% (15 μm), respectively. The increase in apparent density is higher than that in tap density, which is particularly useful for binder jetting due to the relatively loosely packed powder bed.

A similar trend is also seen in the printed green part density (Fig. 2). For example, after mixing 15 μm or 30 μm particles into the 5 μm powder, the printed green part density improves by 3.0–9.4%. While the counter-rotating roller typically densifies the powder in powder bed-based AM processes, Fig. 2 shows that green part density that is lower than the powder apparent density. This can be explained by (i) the inherent inaccuracy in the green density measurement method (Sec. 2.3) and (ii) an insufficient powder compaction effect from recoating.

3.1.3 Powder Flowability. The Hausner ratio (tap density over apparent density) shows the powder flowability in bimodal mixtures noticeably improved over the fine constituent powder (Table 2). The improved flowability is critical in achieving smooth and dense powder layers in the binder jetting process.

3.2 Sintered Density and Shrinkage of Bimodal Powder Mixtures. With a demonstrated benefit in improving green part density and spreading quality, the bimodal powder mixture's impact on sintered density was then explored. Five micrometer powders were mixed with 15 and 30 μm powders at two different mixing ratios (73:27 and 27:73), and then sintered by a sintering profile with a 2-h hold at 1080 °C peak temperature and 2 °C/min heating/cooling rate (Sec. 2.4).

As seen in Fig. 3, there exists a trend in improved sintered density for all bimodal mixtures compared to the 5 μm powder, of which the sintered density is stymied by the low green density (44%) due to the poor powder flowability.

As compared with the fine constituent powder (5 μm), the bimodal powder is capable of improving sintered density while reducing the shrinkage (Fig, 3). While a 40–50% volumetric shrinkage (about 15% linear shrinkage) is normal for binder jetting of metals and can be compensated by scaling the STL file, the reduced shrinkage achieved by bimodal mixtures can provide additional dimensional control for printing high precision parts.

3.3 Influence of Sintering Conditions on Bimodal Powder Mixtures

3.3.1 Effect of Isotherm Temperature and Duration. In order to explore the impact of sintering conditions on bimodal powder mixtures, the authors evaluated three powder mixtures (15 + 5 μm, 75 + 15 μm, and 30 + 5 μm), which were sintered under different heating profiles (Fig. 4), where a peak temperature was held at 1020 °C or 1060 °C for a duration of 30 min or 120 min.

The sintered density and densification were compared across the powder mixtures in each quadrant of Fig. 4. The densification in this result corresponds to the density gain from green density to sintered density. While a powder part typically densifies upon sintering, the 75 + 15 μm powder mixture in Fig. 4(*a*) has shown a slight reduction in density after sintering, due to the strong sintering inhibition effect of the large particles under insufficient sintering conditions and possible part expansion due to debinding outgassing.

Under the least sufficient sintering condition, the powder bed density dominates in determining sintered density, as the sintering densification is limited. For example, when the powder mixtures that contain large particles (e.g., 75 μm) are sintered with the

Table 2 Particle size and density of the powder mixtures

Mixture name	Powder components	Median size (D50)	Standard deviation	Apparent density	Tapped density	Hausner ratio
75	75 μm	77.9 μm	23.2 μm	56.1%	64.9%	1.16
75 + 15	75 μm (73 wt %) + 15 μm	27.0 μm	39.2 μm	59.7%	66.9%	1.12
30	30 μm	26.4 μm	10.9 μm	48.5%	60.8%	1.25
30 + 5	30 μm (73 wt %) + 5 μm	17.4 μm	12.4 μm	53.7%	63.9%	1.19
15	15 μm	17.0 μm	6.7 μm	52.9%	65.1%	1.23
15 + 5	15 μm (73 wt%) + 5 μm	10.8 μm	4.7 μm	54.6%	67.4%	1.23
5 + 30	5 μm (73 wt %) + 30 μm	8.3 μm	15.4 μm	54.4%	61.2%	1.13
5 + 15	5 μm (73 wt %) + 15 μm	5.8 μm	2.7 μm	47.3%	60.5%	1.28
5	5 μm	5.5 μm	N/A	41.7%	55.6%	1.33

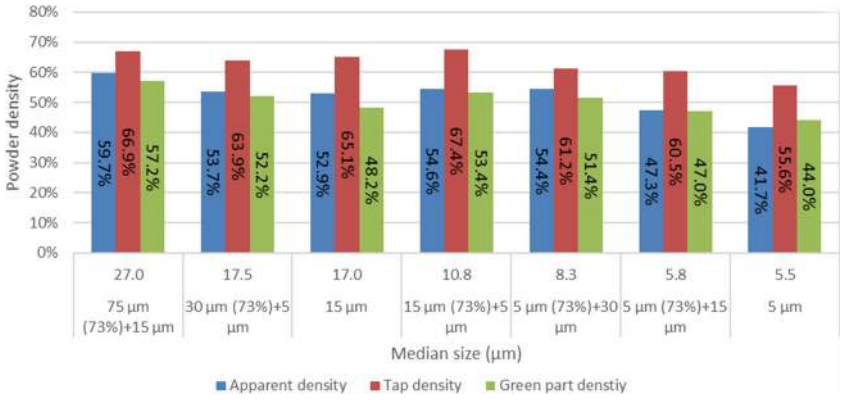

Fig. 2 Comparison of apparent density, tap density, and green density for different powders (see figure online for color)

insufficient condition (Fig. 4(*a*)), the initial green density is most influential on final sintered density. However, when treated with additional energy during sintering (Figs. 4(*b*)–4(*d*)), the high green density in 75 + 15 μm powder parts has failed to generate dense sintered parts as compared to the 15 μm powder.

The powder mixtures without extra coarse powders were able to improve powder bed packing, and green density without dramatically shifting median particle size was effective in improving sintered density. Compared with the 15 μm powder (median size of 17.0 μm), the 30 + 5 μm powder mixture has a similar median particle size (17.4 μm) but a wider distribution, which results in a 4.0% more dense green parts, and a 7.5–11.7% more dense sintered parts depends on the sintering condition (Fig. 4).

3.3.2 Effect of Heating Ramp. The influence of heating/cooling rate on bimodal powder mixtures was studied by sintering loosely packed powders contained in crucibles at 1080 °C for 120 min with different heating rates (Fig. 5). While heating rate is usually associated with facilitating debinding outgassing in sintering powder compacts, this experiment isolated the debinding effect from sintering and solely studied the heating rate's impact on sintered density. It exits a general trend from the result that monosized powders (5, 15, and 30 μm powders) are more sensitive to heating rates than the powder mixtures. For example, 5 μm and 15 μm powders have seen approximately 10% increase in sintered density by lowering heating rate from 5 °C/min to 3 °C/min, while the sintered density of bimodal powder mixtures does not rely on lowering heating rate to achieve maximum density.

Low heating rates provide more energy input into solid state diffusion and provide longer time window that allows particles to rearrange and densify. The authors believe that the improved green density provides more contacting areas among particles and creates a network of particles as a diffusion path in bimodal powder mixtures, which makes it less sensitive to total energy input compared with the monosized powders.

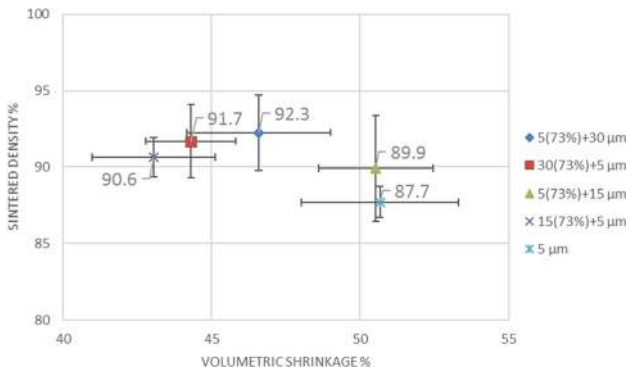

Fig. 3 Sintered density and volumetric shrinkage of 5 μm powder and its bimodal mixtures, sintered at 1080 °C for 2 h

3.4 Microscopic Analysis of Sintered Bimodal Powder Parts. The microstructure of the surfaces in sintered bimodal powder parts were characterized by SEM. Figure 6(*a*) shows that the necking has developed between 15 μm and 75 μm particles, while there is a limited direct necking and merging between 75 μm particles. The sintered part, therefore, is composed of a rigid skeleton of 75 μm particles, wherein the high sintering rate of fine powders has little contribution to the overall densification, which corresponds to the limited densification of the 75 + 15 μm powder in Fig. 4. The 30 + 5 μm powder, on the other hand, has a better densification result through the merging of 30 μm and 5 μm particles into a coherent body (Fig. 6(*b*)). The powder mixture provided more contact points as available neck formation sites and formed an integrated structure by surface reduction.

The sintering advantage of bimodal powders is also evident in the microscopic images of the sectioned and polished sintered parts (Fig. 7). The 30 + 5 μm sintered part has less pores with smaller sizes and a smoother outer surface compared with the 5 μm sintered sample. The sectioned *XY* plane (perpendicular to build orientation) shows pores aligned between the lines of printed primitives. As the binder droplet wets and penetrates powder, the surface tension of the binder typically leads to powder balling and rearrangement of powder particles within the primitive, leaving behind more porosity between primitives, especially in a loosely packed powder.

3.5 Discussion. While prior literature in sintering of compact powders suggests using the fine powder constituent to achieve maximum-sintered density, the results from these sintering trials suggest the maximum sintered density achieved by using the bimodal powder mixtures. This is mostly attributed to the green parts' increased density and small particles' high sintering driving force when bimodal powder mixture is used in binder jetting.

The unique-sintered density improvement of bimodal powders in binder jetting can be also explained using German's prediction model, which states that there exists a critical relationship between the large and small powder shrinkage and the design of powder mixtures for maximum sintered density [13]. In general, when a powder mixture contains small particles with large sintering shrinkage and large particles with small sintering shrinkage, the highest density is achieved by only using the small particles (region A in Fig. 8); when a powder mixture is a combination of small particles with small sintering shrinkage and large particles with large sintering shrinkage, the highest density is achieved with bimodal mixture (region B in Fig. 8).

In binder jetting, the sintering shrinkage of fine powders is usually constrained by the poor powder flowability and low packing

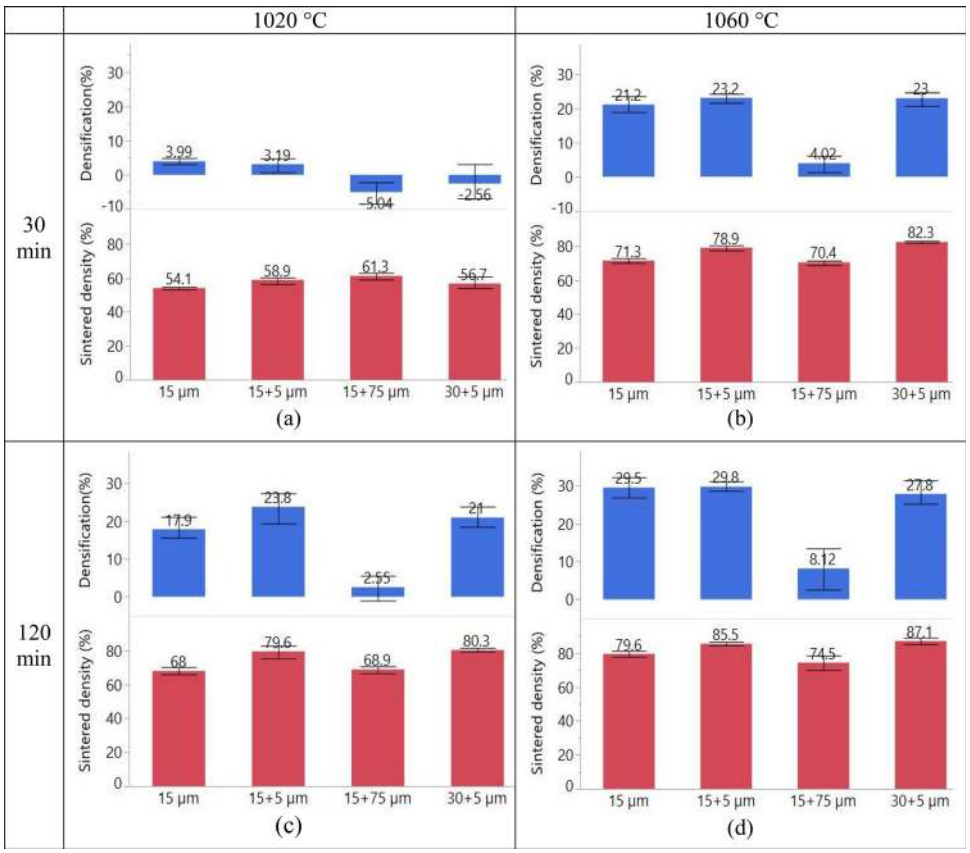

Fig. 4 Sintered density and densification comparison under various sintering conditions (error bars are constructed with the min and max of the data)

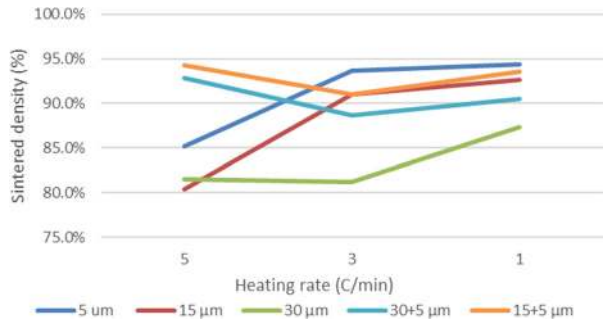

Fig. 5 Sintered density of loosely packed powders in crucible with different heating rates

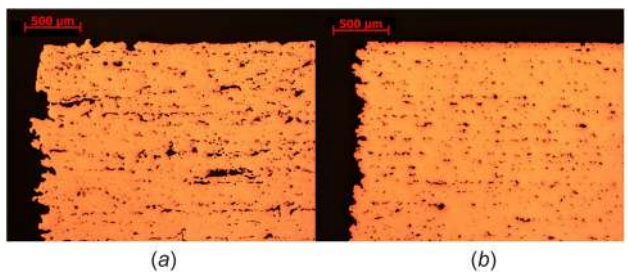

Fig. 7 Optical microscopy of 5 μm powder (left) and 30(73%) + 5 μm powder (right), sintered under the conditions in Sec. 3.2

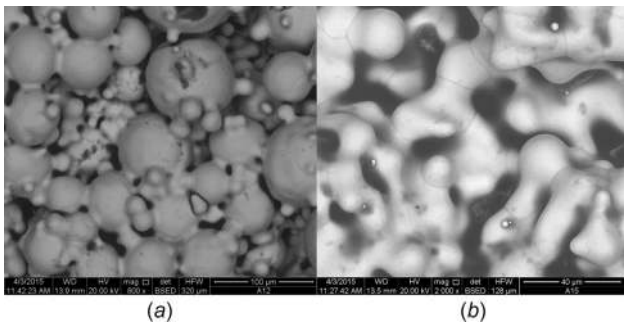

Fig. 6 Surface microstructure of bimodal powder parts sintered at 1060 °C for 120 min: (*a*) 75 + 15 μm powder (800×) and (*b*) 30 + 5 μm powder (2000×)

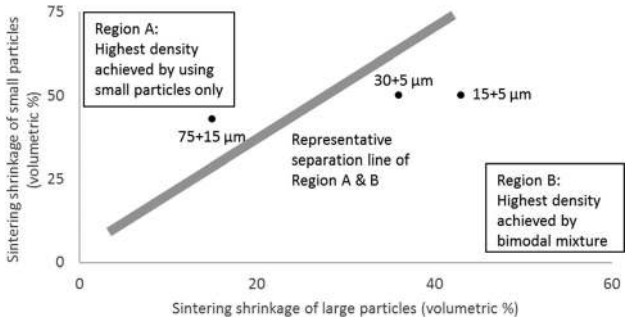

Fig. 8 An illustration of the relationship between the constituent powder shrinkage and the design of powder mixtures for maximum sintered density (the separation line is only representative in this figure and needs to be determined for each powder mixture based on particle size ratios)

density, which makes the bimodal powder to have a stronger tendency to fall in region B. In this work, when 5 μm powder is mixed with 15 μm or 30 μm powder, the sintering shrinkage difference between small and large particles is relatively small, and therefore, the maximum sintered density is achieved by bimodal mixture. When 15 μm powder is mixed with 75 μm, the sintering shrinkage of coarse powder is significantly reduced; therefore, the bimodal powder mixture is not effective at improving sintered density.

As a result, while it is more likely to achieve the maximum sintered density through bimodal powder mixtures in binder jetting than compacted powders, its effectiveness is still affected by many factors, especially, the sintering shrinkage of the constituent powders of the material in question.

4 Conclusion

Several benefits of using bimodal powder mixture in binder jetting of metals have been demonstrated in this work with copper powders. The bimodal powder mixtures have successfully improved powder packing density and powder flowability. As a result, the printed green part density is able to increase by up to 9.4% as compared to the monosized powder counterparts (Fig. 2).

The use of bimodal powder mixtures in binder jetting can also improve sintered density. For example, by replacing the monosized 15 μm powder with the $30+5$ μm powder mixture, the sintered density improved by 12.3% (Fig. 4); However, when large particles (75 μm) were mixed into a fine powder (15 μm), the sintered density was not improved due to the rigid skeleton formed by large particles where the sintering contribution of fine powders is constrained (Fig. 4). The feasibility of improving sintered density by bimodal mixtures over the constituent powders has also been demonstrated by the sintering experiments, however, its effectiveness is complicated by many factors, especially, the particle size ratio and the relative difference in sintered shrinkage of the constituent powders (Sec. 3.5).

In addition to increased sintered density, the use of bimodal powder mixtures shows additional benefits: (i) the shrinkage is reduced due to increased green (see figure online for color) density (Fig. 4); (ii) the bimodal powder mixture is less sensitive to sintering conditions, and potentially can be sintered with less energy input compared to monosized powders (Fig. 5).

There is an opportunity to explore the effects of bimodal powder on additional materials and powder sizes. This work provides (i) an evidence of improved sintered density by bimodal mixture in binder jetting of copper, (ii) an insight on how powder size distribution affects product property in powder bed-based additive manufacturing, and (iii) a framework for powder optimization in order to achieve high sintered density in binder jetting of metals.

Acknowledgment

This material is based upon the work supported by the National Science Foundation under Grant No. #1254287. Any opinions, findings, and conclusions or recommendations expressed in this material are those of the author(s) and do not necessarily reflect the views of the National Science Foundation. The authors acknowledge supports provided by the ExOne Co. Special thanks to Dan Brunermer of ExOne Co., and Carlos Suchicital, Michael Ellis, Jeremy Beach of Virginia Tech, for the discussion and facility support.

References

[1] Mercelis, P., and Kruth, J.-P., 2006, "Residual Stresses in Selective Laser Sintering and Selective Laser Melting," Rapid Prototyping J., **12**(5), pp. 254–265.
[2] Bai, Y., and Williams, C. B., 2015, "An Exploration of Binder Jetting of Copper," Rapid Prototyping J., **21**(2), pp. 177–185.
[3] Zhang, S., Miyanaji, H., Yang, L., Ali, A., and Dilip, J. J. S., 2014, "An Experimental Study of Ceramic Dental Porcelain Materials Using A 3D Print (3DP) Process," Solid Freeform Fabrication Symposium (SFF), Austin, TX, Aug. 4–6, pp. 991–1011.
[4] Chou, D. T., Wells, D., Hong, D., Lee, B., Kuhn, H., and Kumta, P. N., 2013, "Novel Processing of Iron-Manganese Alloy-Based Biomaterials by Inkjet 3-D Printing," Acta Biomater., **9**(10), pp. 8593–8603.
[5] Williams, C. B., Cochran, J. K., and Rosen, D. W., 2011, "Additive Manufacturing of Metallic Cellular Materials Via Three-Dimensional Printing," Int. J. Adv. Manuf. Technol., **53**(1–4), pp. 231–239.
[6] Holman, R. K., 2001, "Effects of the Polymeric Binder System in Slurry-Based Three Dimensional Printing of Ceramics," Ph.D. thesis, Massachusetts Institute of Technology, Cambridge, MA.
[7] Gregorski, S. J., 1996, "High Green Density Metal Parts by Vibrational Compaction of Dry Powder in Three Dimensional Printing Process," Ph.D. thesis, Massachusetts Institute of Technology, Cambridge, MA.
[8] Yoo, J., Cima, M. J., Khanuja, S., and Sachs, E. M., 1993, "Structural Ceramic Components by 3D Printing," Solid Freeform Fabrication Symposium (SFF), Austin, TX, Aug. 9–11, pp. 40–50.
[9] Gaytan, S. M., Cadena, M. A., Karim, H., Delfin, D., Lin, Y., Espalin, D., MacDonald, E., and Wicker, R. B., 2015, "Fabrication of Barium Titanate by Binder Jetting Additive Manufacturing Technology," Ceram. Int., **41**(5), pp. 6610–6619.
[10] Orange, M. J., Kuhn, H. A., Knor, P. P., and Lizzi, T., 2015, "Process for Making Nickel-Based Superalloy Articles by Three-Dimensional Printing," Patent No. WO 2015/183796 A1.
[11] Kernan, B. D., Sachs, E. M., Oliveira, M. a., and Cima, M. J., 2007, "Three-Dimensional Printing of Tungsten Carbide-10 wt% Cobalt Using a Cobalt Oxide Precursor," Int. J. Refract. Met. Hard Mater., **25**(1), pp. 82–94.
[12] Coble, R. L., 1973, "Effects of Particle-Size Distribution in Initial-Stage Sintering," J. Am. Ceram. Soc., **56**(9), pp. 461–466.
[13] German, R. M., 1992, "Prediction of Sintered Density for Bimodal Powder Mixtures," Metall. Trans. A, **23**(5), pp. 1455–1465.
[14] Xiang, Z., Yin, M., Deng, Z., Mei, X., and Yin, G., 2016, "Simulation of Forming Process of Powder Bed for Additive Manufacturing," ASME J. Manuf. Sci. Eng., **138**(8), p. 81002.
[15] Karapatis, N., and Egger, G., 1999, "Optimization of Powder Layer Density in Selective Laser Sintering," International Solid Freeform Fabrication Symposium (SFF), Austin, TX, Aug. 11–13, pp. 255–264.
[16] Zhou, J., Zhang, Y., and Chen, J. K., 2009, "Numerical Simulation of Laser Irradiation to a Randomly Packed Bimodal Powder Bed," Int. J. Heat Mass Transfer, **52**(13–14), pp. 3137–3146.
[17] Spierings, A. B., Herres, N., Levy, G., and Buchs, C., 2010, "Influence of the Particle Size Distribution on Surface Quality and Mechanical Properties in Additive Manufactured Stainless Steel Parts," International Solid Freeform Fabrication Symposium (SFF), Austin, TX, Aug. 9–11, pp. 397–406.
[18] Lanzetta, M., and Sachs, E., 2003, "Improved Surface Finish in 3D Printing Using Bimodal Powder Distribution," Rapid Prototyping J., **9**(3), pp. 157–166.
[19] Verlee, B., Dormal, T., and Lecomte-Beckers, J., 2011, "Properties of Sintered Parts Shaped by 3D-Printing From Bimodal 316L Stainless Steel Powder Mixtures," EURO PM2011 Congress & Exhibition, Barcelona, Spain, Oct. 9–12, pp. 357–362.
[20] Utela, B., Storti, D., Anderson, R., and Ganter, M., 2008, "A Review of Process Development Steps for New Material Systems in Three Dimensional Printing (3DP)," J. Manuf. Process., **10**(2), pp. 96–104.
[21] Zheng, J., Carlson, W. B., and Reed, J. S., 1995, "The Packing Density of Binary Powder Mixtures," J. Eur. Ceram. Soc., **15**(5), pp. 479–483.